Progress In Electromagnetics Research, Vol. 108, 37–49, 2010

PERFECT METAMATERIAL ABSORBER WITH DUAL BANDS

M.-H. Li, H.-L. Yang, and X.-W. Hou

College of Physical Science and Technology
Huazhong Normal University
Wuhan 430079, China

Y. Tian

Department of Electronics and Information Engineering
Huazhong University of Science and Technology
Wuhan 430074, China

D.-Y. Hou

National Key Laboratory of EMC
China Ship Industry Corporation No. 701 Research and Development Institute
Wuhan 430064, China

Abstract—In this paper, we present the design, simulation, and measurement of a dual-band metamaterial absorber in the microwave region. Simulated and experimental results show that the absorber has two perfect absorption points near 11.15 GHz and 16.01 GHz. Absorptions under different polarizations of incident EM waves are measured with magnitude of over 97% at low-frequency peak and 99% at high-frequency peak respectively. Current distribution at the dual absorptive peaks is also given to study the physical mechanism of power loss. Moreover, it is verified by experiment that the absorptions of this kind of metamaterial absorber remain over 90% at the low-frequency peak and 92% at the high-frequency peak with wide incident angles ranging from 0° to 60° for both transverse electric wave and transverse magnetic wave.

Received 14 July 2010, Accepted 2 September 2010, Scheduled 9 September 2010
Corresponding author: H.-L. Yang (emyang@mail.ccnu.edu.cn).

1. INTRODUCTION

Metamaterials (MMs) are artificial effectively homogeneous electromagnetic structures composed of metals and dielectrics. The initial impetus driving metamaterial research was the realization of effective negative permittivity, permeability and refractive index [1–4]. Since the experimental demonstration of negative refractive index in the left-handed metamaterials (LHMs) by Smith [5], MMs research has attracted intense attention of the scientific community. As a new type of artificial materials, it can be applied to many disciplines, such as filter, waveguide, resonator and antenna [6–9]. To date, MMs have been demonstrated in every spectral range, from radio [10], microwave [4], mm-wave [11], THz [12], MIR [13], NIR [14], and even near optical [15]. Most of the MMs are made of periodically arranged metallic structures much smaller than the working wavelength in size. The electromagnetic responses of MMs can be characterized as homogeneous media, and the permittivity, permeability, refractive index and impedance can be tailored through the design of unit cells of the MMs. The major advantage of MMs over natural materials is that the macroscopic parameters can be designed to have desired values. Meanwhile, the wave absorption property of metamaterials has been nearly neglected. By adjusting the refraction and impedance of the MMs, a "perfect" absorber with near-unity absorption can be realized which is called resonant metamaterial absorber (MMA). Quite recently, there has been considerable interest in creating resonant metamaterial absorbers through tailorable design of refractive index and impedance.

Due to the diffraction limit, the thickness of conventional absorbers cannot be made thin enough, so the reduction of the electrical thickness of the absorber is one of the challenging aspects in designing such components. As an effective medium [16], MMs can be characterized by a complex electric permittivity $\varepsilon(\omega) = \varepsilon_1(\omega) + i\varepsilon_2(\omega)$ and magnetic permeability $\mu(\omega) = \mu_1(\omega) + i\mu_2(\omega)$. Just as left-handed metamaterials, most attention was focused on the real part of permittivity and permeability to realize negative refractive material. However, by carefully designing the unit cell structures, both the real and imaginary parts could be tailored so as to exhibit desired electromagnetic features. For resonant metamaterial absorber (MMA), the idea is to make the impedance of absorber $Z(\omega) = \sqrt{\mu(\omega)/\varepsilon(\omega)}$ match to that of free space and possess a large imaginary part of refraction index $n(\omega) = \sqrt{\varepsilon(\omega)\mu(\omega)}$ simultaneously. Therefore, both the transmission and reflectivity are minimized due to the impedance matching and large losses in the absorber and the incident energy will be converted into heat.

Landy et al. proposed a perfect metamaterial absorber with absorption of 96% in simulation and 88% in experiment at around 11.5 GHz [17]. After that, other approaches have been theoretically put forward to extend these ideas to higher frequencies [18, 19] or to increase the band width of the absorption. A highly flexible wide angle of incidence terahertz metamaterial absorber was proposed by Tao et al. [20]. Rozanov gives a fundamental limit on how good an absorber can be [21] and a simple, fast and efficient method for designing wide-band radar absorbers is studied by Zadeh et al. The method is a modification of the circuit analog absorber with simple design and fabrication process which make great contributions on this subject [22]. However, most meatamaterial absorbers are one-dimensional structure. To combine well with applications, polarization-insensitive and wide-angle metamaterial absorber is experimentally demonstrated [23–26]. Dual band terahertz metamaterial absorber is reported by Wen et al. [27]. The results show that the one-dimensional absorber has two distinct absorption points near 0.45 and 0.92 THz. MMA hold great promise for future applications such as bolometer, invisibility cloaks, sub-wavelength imaging and so on [28–31].

In this paper, perfect metamaterial absorber with dual bands at microwave frequency is presented. The impedance of the MMA is designed to match that of free space at around 11.15 and 16.01 GHz. Simulated and experimental results are is good agreements which demonstrate two perfect absorption peaks. Current distribution at the dual absorptive peaks is also given to study the physical mechanism of power loss. Experiments are carried out to explore the absorbing characteristics for different polarizations of normal incident EM waves. Moreover, absorptions with different oblique incident angles (for both TE and TM modes) are investigated in experiments which verify the nearly perfect absorption of the proposed design.

2. DESIGN OF EXPERIMENTS AND SIMULATIONS

A compact metamaterial absorber consists of two metallic layers. The perspective view of a single unit cell of the MMA is shown in Fig. 1(b) which composes of 2×2 array of eSRRs oriented in different directions. Fig. 1(a) is the front view of the single electric split-ring resonator. The inner radius is $r_2 = 2.3$ mm and the outer radius is kept to $r_1 = 2.7$ mm. The width of the wires and the capacitor gap are all kept to $w = 0.2$ mm. The length of the middle capacitor is $l = 1.6$ mm. These were fabricated on top layer of the FR-4 circuit board. The bottom of the FR-4 circuit board is metal plate as Fig. 1(b) shows. The two metallic layers are separated by a dielectric spacer

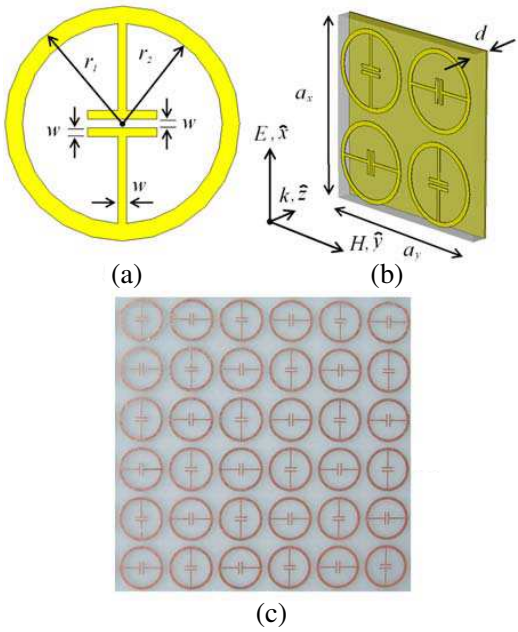

Figure 1. (a) Front view of the single electric split-ring resonator (eSRR). (b) Perspective view of the one unit cell. (c) Photograph of a portion of the experimentally realized absorber (top layer). The single eSRR next to the other is rotated with 90 degree and all of them are crossed displayed on the top side.

with $d = 0.5\,\text{mm}$ and the relative dielectric constant is kept to 4.1. The designed MMA was fabricated into a 25×25 unit cells sample ($300\,\text{mm} \times 300\,\text{mm} \times 0.56\,\text{mm}$) with lattice spacing $a_x = a_y = 12\,\text{mm}$ by means of printed-circuit-board technology. To date, the single eSRR next to the other is rotated with 90 degree and all of them are crossed displayed on the top side as Fig. 1(c) shows. This unique arrangement plays an important part in yielding perfect metamaterial absorber with dual bands. The eSRRs at the front side of FR-4 board is primarily responsible for determining $\varepsilon(\omega)$, while the bottom metallic layer is designed such that the incident magnetic field drives circulation currents between the two layers.

The absorption is calculated by $A = 1 - |S_{11}|^2 - |S_{21}|^2$. In both simulations and experiments, we only need the reflection to calculate the absorption because there would be no transmission through the absorber across the entire frequency range due to the shielding of the

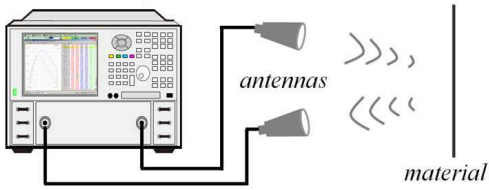

Figure 2. Schematic of reflection measurement. The two horn antennas serving as the source and receiver are connected to a network analyzer with low loss flexible cables.

bottom metal plate.

In the simulations, the reflection coefficients from a single unite cell with periodic boundary condition is obtained with CST Microwave Studio (High frequency electro-magnetic simulation software which is based on Finite Integration Time Domain method). EM waves propagate along the z direction (The microwaves were incident normal to the sample surface). The electric field polarization is kept along the x axis, and magnetic field polarization is kept along the y axis.

In the experiments, reflection properties of the MMA are performed in Microwave Anechoic Chambers which allows us to use without any restrictions on the size of the structures. Fig. 2 is the schematic of reflection measurement. A pair of horn antennas serving as the source and receiver was connected to an Agilent E8361B network analyzer with low loss flexible cables. The two antennas should be placed on the same side of the sample and the reflection measurements were calibrated using a sample-sized sheet of copper as a reflecting mirror. Microwave absorbing material is placed surrounding the sample sheet to eliminate the unwanted edge scattering. The height of the horn antennas is kept to be 2 m and the distance between horns and material is 0.5 m to get rid of near field effects. We first give the reflection and absorption properties with the material under normal incidence and the electric field polarization is kept along the x axis as Fig. 1(a) shows. The absorption properties with different polarizations and varied incident angles are followed, as will be discussed in more detail below.

The simulated and measured reflection as a function of frequency under normal incidence with electric field polarized along x axis is presented in Fig. 3 and Fig. 4, and the frequency characteristic of absorption can be calculated by $A = 1 - |S_{11}|^2$ ($S_{21} = 0$ due to the shielding of the bottom metal plate) as the dash lines show. It can be observed that the reflection of the absorber drops to a minimum at both

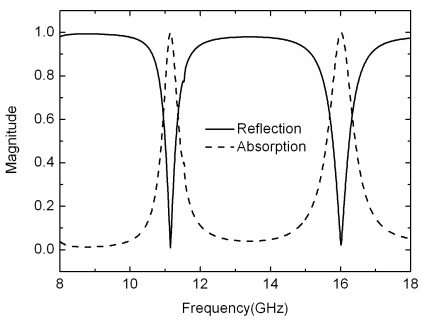

Figure 3. Simulated reflection and absorption as a function of frequency under normal incidence with electric field polarized along x axis.

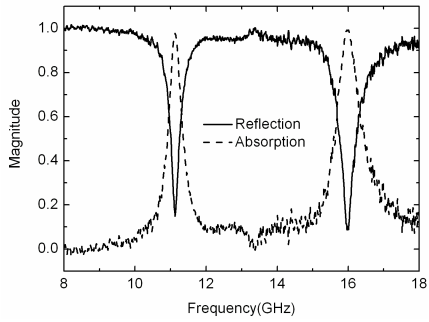

Figure 4. Measured reflection and absorption as a function of frequency under normal incidence with electric field polarized along x axis.

frequency of 11.15 GHz and 16.01 GHz denoting impedance matching with the free space. Accordingly, there are two distinct absorptive peaks, each with absorption over 99.99%. The absorption bandwidths, defined as full width at half maximum, are 0.32 GHz and 0.62 GHz for the low-frequency and high-frequency peak respectively. As can be seen from above, perfect absorption only occurs with very narrow band at resonant frequency. At around the frequency from 8 GHz to 11 GHz, 12 GHz to 15 GHz and 17 GHz to 18 GHz, the absorption is less than 20%. After all, experimental and simulated results are in great agreements.

$$\tilde{z}(\omega) = \sqrt{\frac{(1+S_{11})^2 - S_{21}^2}{(1-S_{11})^2 - S_{21}^2}}$$

From above retrieved equation, both the real and imaginary part of relative wave impedance is shown in Fig. 5. At the absorptive peaks of frequency 11.15 GHz and 16.01 GHz, the real relative impedance is near unity, $\mathrm{Re}(\tilde{z}) \approx 1$, which means $\tilde{z} \approx \tilde{z}_0$ (Where $\tilde{z}_0$ is the impedance of the free space) and the imaginary part is minimized, $\mathrm{Im}(\tilde{z}) \approx 0$, such that the reflection is nearly zero.

To better understand the physical mechanism of the dual-band metamaterial absorber, current distribution on the metals and the distribution of power-loss were plotted in Fig. 6 and Fig. 7. We first discuss the low-frequency case at 11.15 GHz. Fig. 6 shows that the eSRR2 (The center capacitor plates are parallel to the electric field) have very strong surface current which is responsible for the

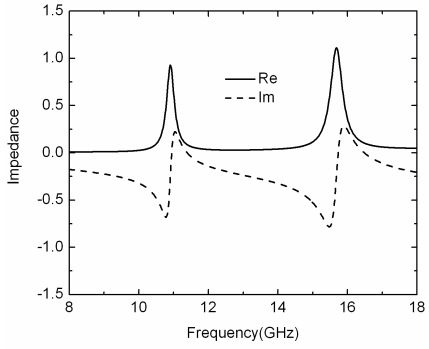

Figure 5. Real part (solid line) and imaginary part (dashed line) of relative impedance extracted from simulations.

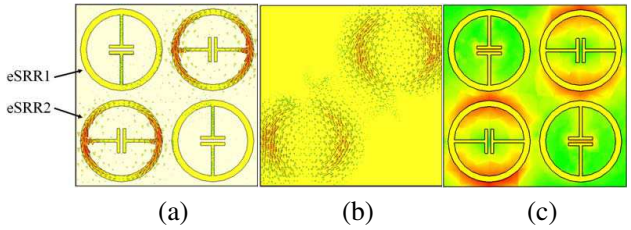

Figure 6. (a) Simulated surface currents on the front eSRRs and (b) back metallic plate at the frequency of 11.15 GHz. (c) A bird-view for the distribution of the power-loss (absorption) at the frequency of 11.15 GHz.

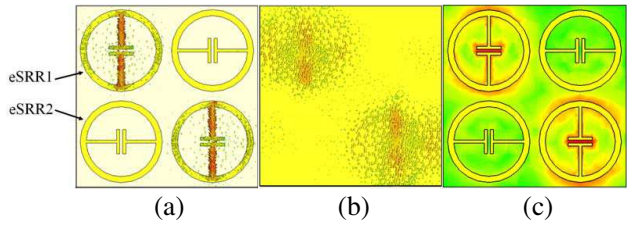

Figure 7. (a) Simulated surface currents on the front eSRRs and (b) back metallic plate at the frequency of 16.01 GHz. (c) A bird-view for the distribution of the power-loss (absorption) at the frequency of 16.01 GHz.

low-frequency absorption. Current at the two sides of the ring is strong associated with a dipolar response which contributes to the effective $\varepsilon(\omega)$ [20]. There is also a magnetic response associated with a circulating displacement current between the two metallic

elements [24]. As Fig. 6(c) shows, most of the power loss takes place in the upper and lower parts of the ring and dielectric losses occur in between the two metallic plates where the electric field is large [17]. However, things are much different for high-frequency case. Currents are strong in the place of eSRR1 (The center capacitor plates are perpendicular to the electric field). Strong currents accumulate at the center bar which works as a dipolar response. It is also observed that currents are flowing in opposite directions along x axis owing to the magnetic flux between the two metallic plates along y axis. In Fig. 7(c), we can see the power losses occur at the center capacitor and the upper and lower parts of the ring. As said above, in order to couple to the incident H-field, we needed flux created by circulating charges perpendicular to the propagation vector and the thickness of the dielectric layer is very important in tuning the effective μ. By carefully manipulating the electric and magnetic coupling, we can make the impedance of absorber $Z(\omega) = \sqrt{\mu(\omega)/\varepsilon(\omega)}$ match to that of free space at last.

3. EXPERIMENTAL VERIFICATION

To demonstrate the polarization insensitivity of the absorber sheet, the horns are rotated for different angles around the main radiation direction to generate and receive EM waves with different polarizations. Because the single unit cell next to the other is rotated with 90 degree and all of them are crossed displayed as Fig. 1(c) shows, angles from 0° to 45° are enough to verify the insensitive-polarization absorber. Fig. 8 gives absorptions under different polarizations of incident EM waves in the normal incidence case. It is observed from Fig. 8, the absorptions remain greater than 97% for the low-frequency peak with bandwidth of larger than 0.31 GHz. When taking into account the small shift in the center frequency for the high-frequency peak (As angles increased, the absorption peaks drift to low frequency with magnitude of 0.11 GHz from 0° to 45°), the absorption at the peak frequency is still more than 99%, which verifies the nearly perfect absorption and polarization insensitivity of the proposed design.

In the above section, we have just obtained the absorption under normal incidence. In practical uses, EM waves are usually incident onto absorbers with an oblique incidence angle, so it is necessary to get the absorption with an oblique incidence. Fig. 9 and Fig. 10 show the measured absorptions for TE and TM waves with an oblique incident angle ranging from 0° to 60°. For incident angle larger than 60°, the measurement will be affected by the unavoidable direct coupling between the two horns in the experimental setup, so that the absorbing

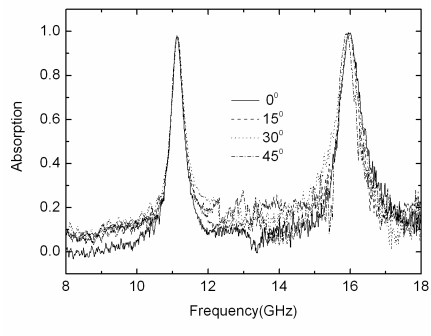

Figure 8. Measured absorptions under different polarizations of incident EM waves in the normal incidence case. The labels for the curves show the angles between the electric vector and the x axis.

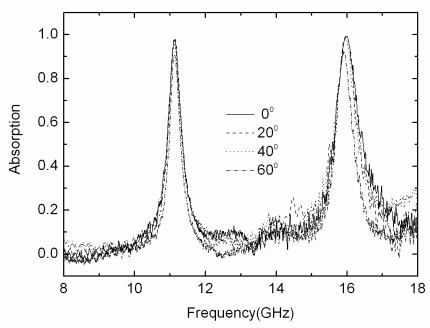

Figure 9. Measured absorptions at different oblique incident angles for TE mode. The labels for different curves indicate the incident angles.

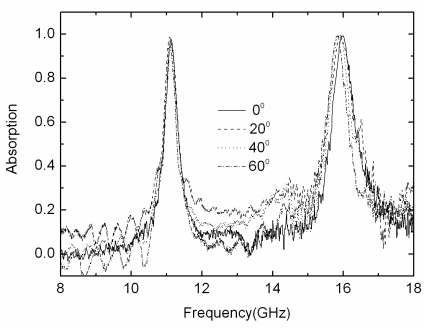

Figure 10. Measured absorptions at different oblique incident angles for TM mode. The labels for different curves indicate the incident angles.

characteristics for larger oblique angles are not obtained. It is observed from Fig. 9 that for TE waves, as the incidence angles increase, the maximum absorption decreases slightly for both the low-frequency and high-frequency peaks. For incident angle of 60°, the peak absorption drops to 90% at low-frequency peak and 92% at high-frequency peak. This can be explained that incident magnetic field can no longer efficiently induce the resonant currents on the front and back metallic plates. For TM polarization, the absorption is almost unity and remains above 94% for low-frequency peak and 99% for high-frequency peak. There is also a slight frequency shift of less than 0.16 GHz from

0° to 60° at high-frequency peak. In this case, the magnetic field can efficiently drive the circulating currents at all angles of incidence which is important to maintain impedance matching. Since any oblique incident EM waves can be decomposed into TE and TM modes, these measurement results indicate that the proposed absorber can work well for oblique incident EM waves over a large range of incident angles.

4. CONCLUSION

In summary, a polarization-insensitive and wide-angle metamaterial absorber with dual bands has been successfully fabricated and tested. To better understand the physical mechanism of the dual-band metamaterial absorber, current distribution on the metals and the distribution of power-loss were plotted. Absorptions under different polarizations of incident EM waves are measured with magnitude of over 97% at low-frequency peak and 99% at high-frequency peak respectively. Moreover, the measurement results with wide incident angle ranging from 0° to 60° are given. The absorptions remain over 90% at the low-frequency peak and 92% at the high-frequency peak for both transverse electric wave and transverse magnetic wave. With geometrical scalability, this dual-band metamaterial absorber could realize at other frequency range with nearly perfect absorption. These metamaterials have great promise for future applications such as bolometer, EM wave spatial filter, etc.

REFERENCES

1. Veselago, V. G., "The electrodynamics of substances with simultaneously negative values of ε and μ," *Sov. Phy. Usp*, Vol. 10, No. 4, 509–514, 1968.
2. Xi, S., H. Chen, B.-I. Wu, and J. A. Kong, "Experimental confirmation of guidance properties using planar anisotropic left-handed metamaterial slabs based on S-ring resonators," *Progress In Electromagnetics Research*, Vol. 84, 279–287, 2008.
3. Zhou, H., Z. Pei, S. Qu, S. Zhang, J. Wang, Q. Li, and Z. Xu, "A planar zero-index metamaterial for directive emission," *Journal of Electromagnetic Waves and Applications*, Vol. 23, No. 7, 953–962, 2009.
4. Ramprecht, J., M. Norgren, and D. Sjoberg, "Scattering from a thin magnetic layer with a periodic lateral magnetization: Application to electromagnetic absorbers," *Progress In Electromagnetics Research*, Vol. 83, 199–224, 2008.

5. Shelby, R. A., D. R. Smith, and S. Schultz, "Experimental verification of a negative index of refraction," *Science*, Vol. 292, 77–79, 2001.
6. Sabah, C. and S. Uckun, "Multilayer system of lorentz/drude type metamaterials with dielectric slabs and its application to electromagnetic filters," *Progress In Electromagnetics Research*, Vol. 91, 349–364, 2009.
7. Si, L.-M. and X. Lv, "CPW-FED multi-band omni-directional planar microstrip antenna using composite metamaterial resonators for wireless communications," *Progress In Electromagnetics Research*, Vol. 83, 133–146, 2008.
8. Khalilpour, J. and M. Hakkak, "S-shaped ring resonator as anisotropic uniaxial metamaterial used in waveguide tunneling," *Journal of Electromagnetic Waves and Applications*, Vol. 23, No. 13, 1763–1772, 2009.
9. Hwang, R.-B., H.-W. Liu, and C.-Y. Chin, "A metamaterial-based e-plane horn antenna," *Progress In Electromagnetics Research*, Vol. 93, 275–289, 2009.
10. Wiltshire, M. C. K., J. B. Pendry, I. R. Young, D. J. Larkman, D. J. Gilderdale, and J. V. Hajnal, "Microstructured magnetic materials for RF flux guides in magnetic resonance imaging," *Science*, Vol. 291, 849–851, 2001.
11. Gokkavas, M., K. Guven, I. Bulu, K. Aydin, R. S. Penciu, M. Kafesaki, C. M. Soukoulis, and E. Ozbay, "Experimental demonstration of a left-handed metamaterial operating at 100 GHz," *Phys. Rev. B*, Vol. 73, 193103-1–193103-5, 2006.
12. Lin, X. Q., T. J. Cui, Y. Fan, and X. Liu, "Frequency selective surface designed using electric resonant structures in terahertz frequency bands," *Journal of Electromagnetic Waves and Applications*, Vol. 23, No. 1, 21–29, 2009.
13. Linden, S., C. Enkrich, M. Wegener, J. F. Zhou, T. Koschny, and C. M. Soukoulis, "Magnetic response of metamaterials at 100 Terahertz," *Science,* Vol. 306, 1351–1353, 2004.
14. Zhang, S., W. J. Fan, N. C. Panoiu, K. J. Malloy, R. M. Osgood, and S. R. J. Brueck, "Experimental demonstration of near-infrared negative-index metamaterials," *Phys. Rev. Lett.*, Vol. 95, 137404-1–137404-5, 2005.
15. Dolling, G., M. Wegener, C. M. Soukoulis, and S. Linden, "Negative-index metamaterial at 780 nm wavelength," *Opt. Lett.*, Vol. 32, 53–55, 2007.
16. Chamaani, S., S. A. Mirtaheri, M. Teshnehlab, M. A. Shooredeli,

and V. Seydi, "Modified multi-objective particle swarm optimization for electromagnetic absorber design," *Progress In Electromagnetics Research*, Vol. 79, 353–366, 2008.

17. Landy, N. I., S. Sajuyigbe, J. J. Mock, D. R. Smith, and W. J. Padilla, "Perfect metamaterial absorber," *Phys. Rev. Lett.*, Vol. 100, 2074021–2074024, 2008.
18. Avitzour, Y., Y. A. Urzhumov, and G. Shvets, "Wide-angle infrared absorber based on a negative-index plasmonic metamaterial," *Phys. Rev. B*, Vol. 79, 045131, 2009.
19. Hao, J., J. Wang, X. Liu, W. J. Padilla, L. Zhou, and M. Qiu, "High performance optical absorber based on a plamonic meamaterial," *Appl. Phys. Lett*, Vol. 96, 251104, 2010.
20. Tao, H., C. M. Bingham, A. C. Strikwerda, D. Pilon, D. Shrekenhamer, N. I. Landy, K. Fan, X. Zhang, W. J. Padilla, and R. D. Averitt, "Highly flexible wide angle of incidence terahertz metamaterial absorber: Design, fabrication, and characterization," *Phys. Rev. B*, Vol. 78, 241103(R), 2008.
21. Rozanov, K. N., "Ultimate thickness to bandwidth ratio of radar absorbers," *IEEE Transactions on Antennas and Propagation*, Vol. 8, No. 48, 1230–1234, 2000.
22. Kazemzadeh, A. and A. Karlsson, "Capacitive circuit method for fast and efficient design of wideband radar absorber," *IEEE Transactions on Antennas and Propagation*, Vol. 57, No. 8, 2307–2314, 2009.
23. Wang, B., T. Koschny, and C. M. Soukoulis, "Wide-angle and polarization-independent chiral metamaterial absorber," *Phys. Rev. B*, Vol. 80, 0331081–0331083, 2009.
24. Zhu, B., Z. Wang, C. Huang, Y. Feng, J. Zhao, and T. Jiang, "Polarization insensitive metamaterial absorber with wide incident angle," *Progress In Electromagnetics Research*, Vol. 101, 231–239, 2010.
25. Lagarkov, A. N, V. N. Kisel, and V. N. Semenenko, "Wide-angle absorption by the use of a metamaterial plate," *Progress In Electromagnetics Research Letters*, Vol. 1, 35–44, 2008.
26. Wang, J. F., S. B. Qu, Z. T. Fu, H. Ma, Y. M. Yang, X. Wu, X. Xu, and M. J. Hao, "Three-dimensional metamaterial microwave absorbers composed of coplanar magnetic and electric resonators," *Progress In Electromagnetics Research Letters*, Vol. 7, 15–24, 2009.
27. Wen, Q. Y., H. W. Zhang, Y. S. Xie, Q. H. Yang, and Y. L. Liu, "Dual band terahertz metamaterial absorber: Design, fabrication, and characterization," *Appl. Phys. Lett.,* Vol. 95, 241111-1–

241111-3, 2009.

28. Han, T. C., X. H. Tang, and F. Xiao, "The petal-shaped cloak," *Journal of Electromagnetic Waves and Applications*, Vol. 23, No. 14–15, 2055–2062, 2009.
29. Luo, Y., J. Zhang, H. Chen, B.-I. Wu, and L.-X. Ran, "Wave and ray analysis of a type of cloak exhibiting magnified and shifted scattering effect," *Progress In Electromagnetics Research*, Vol. 95, 167–178, 2009.
30. Cheng, Q., W. X. Jiang, and T.-J. Cui, "Investigations of the electromagnetic properties of three-dimensional arbitrarily-shaped cloaks," *Progress In Electromagnetics Research*, Vol. 94, 105–117, 2008.
31. Zhao, J., Y. Feng, B. Zhu, and T. Jiang, "Sub-wavelength image manipulating through compensated anisotropic metamaterial prisms," *Opt. Express*, Vol. 16, 18057–18066, 2008.